PCCP

Accepted Manuscript

ROYAL SOCIETY OF CHEMISTRY

www.rsc.org/pccp

Prediction of topological phase transition in X2-SiGe monolayers

Rosalba Juarez-Mosqueda[1]*, Yandong Ma[1]* and Thomas Heine[1,2]*

[1]Department of Physics & Earth Sciences, Jacobs University Bremen, Campus Ring 1, 28759 Bremen, Germany

[2]Lehrstuhl für Theoretische Chemie, Wilhelm-Ostwald-Institut für Physikalische und Theoretische Chemie, Universität Leipzig, Germany

Corresponding author: rjuarezmos@googlemail.com (R.J.M.), myd1987@gmail.com (Y.M.), thomas.heine@uni-leipzig.de (T.H.)

Abstract

Quantum spin Hall (QSH) insulators exhibit a bulk insulting gap and metallic edge states characterized by nontrivial topology. Here, we used first-principles calculations to investigate the electronic and topological properties of halogenated silicon germanide (X2-SiGe, with X = F, Cl, and Br) monolayers, which we found to be trivial semiconductors with energy band gaps ranging from 500 meV to 900 meV. Interestingly, we found that under 8% strain, X2-SiGe monolayers behave as QSH insulators with global band gaps between 53 meV and 123 meV. The underlying mechanism of the topological phase transition is the strain-induced *s-p* band inversion. The nontrivial topological features for the strained X2-SiGe monolayers were further confirmed by the presence of topologically protected edge states that form a single Dirac cone in the middle of the bulk band gaps. Therefore, our results reveal that this new family of QSH insulators is promising for room temperature applications in spintronics and quantum computation devices.

Introduction

Topological insulators (TIs) is a term used to describe those materials that are characterized by a bulk band gap and metallic surface or edge states.[1–4] Two-dimensional (2D) systems that display this phenomenon are known as quantum spin Hall (QSH) insulators. In QSH insulators, the spin of the electrons, rather than the electric charge, is responsible for carrying the electronic information. Therefore, this new class of unconventional materials holds a promising potential for applications in quantum electronic devices and spintronics.[5,6] The QSH effect was firstly predicted in graphene.[4] However, soon after, it was found that the spin orbit coupling (SOC) in graphene is too weak (4 meV) to produce an observable QSH effect under realistic conditions.[7] Up to date, only a few QSH insulators have been observed experimentally, namely, HgTe/CdTe[8] and InAS/GaSb[9] quantum wells, and Bi thin films.[10–16] However, the great majority of these QSH insulators operate only under very low temperature (below 100 K) due to their small band gaps. Therefore, in the last years an extensive effort has been devoted to search for new QSH insulators with large bulk band gaps. Examples include pure or functionalized bismuth,[17–20] antimony,[20] lead,[20] and tin[21] films, gemanene,[21–25] silicene,[21,23] and transition metal dichalcogenides.[26] Among them, QSH insulators that contain elements from the Group 14, such as germanene and stanene, have the advantage that they can be easily integrated into Si-based nanoelectronics, which makes them promising candidates for constructing novel spintronic devices.[27] On the other hand, pure Ge-and Sn-monolayers are unstable under ambient conditions due to the 4-fold coordination of these elements that tends to adsorb foreign atoms or molecules. This is the reason why only functionalized germanene and substrate-supported (*i.e.*, no free-standing) stanene have been synthesized so far.[28–31] Recently, Zhou *et. al*.,[32] have proposed that the stability of germanene can be improved by incorporating Si into the structure. Using first-principles calculations, the authors predicted the dynamical stability of isolated SiGe (silicon gemanide) monolayer. They calculated the electronic band structure of this new 2D SiGe material, which was found to be characterized by Dirac cones at K point.[32] Moreover, it has been proposed that, as in the case of silicene and germanene,[33,34] the electronic band structure of this binary SiGe compound can be strategically tune by hydrogenation.[32] Based on this idea, we studied the electronic band structure of functionalized silicon germanide (SiGe) honeycomb films. We principally focused on

halogenated X2-SiGe monolayers in which X = F, Cl or Br. The X2-SiGe systems with X = H and X = I were also studied and the results are reported in the supporting information (SI). We found that functionalizing the SiGe monolayer with halogen (and H) atoms increases significantly its stability. Moreover, the formation of the X-Si and X-Ge bonds breaks the degeneracy of the π-π^* interactions predicted for the bare SiGe monolayer, which results in an opening of a direct band gap at the Γ point. Interestingly, we found that this band gap is tunable by applying mechanical strain. A SOC-induced global band gap between 53-123 meV closes and then reopens for all X2-SiGe systems under reasonable strain. Moreover, the typical *s-p* band inversion was obtained for all the strained systems. In addition, the existence of conducting edge states connecting the conduction and valence band by a unique Dirac point was confirmed, which demonstrate a topological phase transition in the strained 2D X2-SiGe materials. Furthermore, the SOC-induced nontrivial band gaps in these systems are significantly larger than k_BT at room temperature, which opens the possibility to use these materials in the creation of spintronics and quantum computation devices[6] operating at practical conditions.

Methods

First-principles calculations were carried out using the generalized gradient approximation (GGA) to the density functional theory (DFT)[35–37] within the projector-augmented-wave (PAW) method[38] as implemented in the Vienna Ab-Initio Simulation Package (VASP).[38,39] For the X2-SiGe ground state structures, the atomic positions and lattice vectors were fully optimized until the residual forces were less than 10^{-2} eV Å^{-1}. The kinetic energy cutoff was set to 450 eV with a self-consistency convergence criterion of 10^{-5} eV. The effect of the SOC was included in the self-consistent electronic structure calculations. A Monkhorst-Pack grid[40] of 8 x 8 x 1 was used. The vacuum space between neighboring slabs was set to be > 20 Å. Phonon calculations were performed using the Quantum Espresso code[41] with the PAW potentials that consider 4, 14, and 7 valence electrons for Si, Ge and X (with X = F, Cl, Br) respectively.

Results and Discussion

The optimization of the four-member hexagonal X2-SiGe lattice results into a buckled structures with a relative vertical displacement between Si and Ge (δ) of about 0.7 Å (see **Figure 1**). In these 2D X2-SiGe materials, one halogen atom is bonded to Ge with a distance of 1.79 Å (F-Ge), 2.19 Å (Cl-Ge) and 2.35 Å (Br-Ge), while, on the opposite side, a second one is bonded to Si with bond length of 1.63 Å (F-Si), 2.08 Å (Cl-Si) and 2.25 Å (Br-Si) (see **Figure 1** and **Table 1**). For all the cases, the Si-Ge atoms are sandwiched between the two halogen elements, and the Si-Ge bond distance is ~2.45 Å. The optimized lattice parameters are $a=b$= 4.099 Å, $a=b$= 4.068 Å, and $a=b$= 4.089 Å, for F2-SiGe, Cl2-SiGe and Br2-SiGe respectively. The optimization of I2-SiGe and H2-SiGe was also carried out and the results are shown in SI.

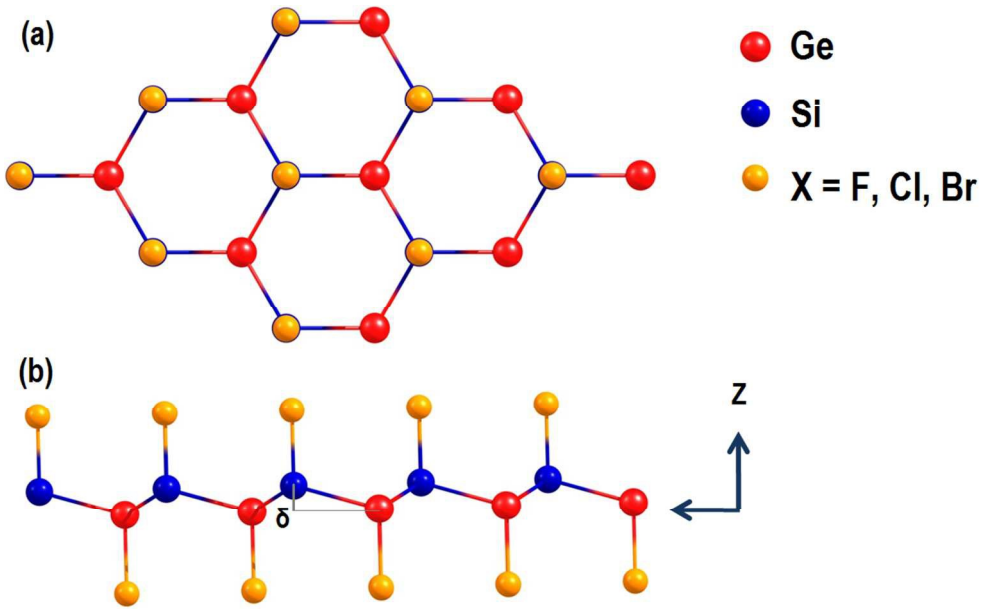

Figure 1. Schematic representation of **(a)** top and **(b)** side views of X2-SiGe (X = F, Cl, Br) monolayers. δ indicates the relative displacement of Si with respect to Ge along the **z**-axis.

Table 1. Si-X and Ge-X bond distances (in Å), lattice parameters *a* and *b* (in Å), and formation energy, ΔE (in eV per unit cell) of X2-SiGe monolayers. ΔE is calculated for the SiGe + X_2→X2-SiGe reaction.

	X = F	X = Cl	X = Br
Si-X	1.63	2.08	2.25
Ge-X	1.79	2.19	2.35
a=*b*	4.099	4.068	4.089
ΔE	-7.324	-3.728	-3.050

The buckled shape of the honeycomb SiGe structure results from the sp^3–hybridization tendency of the Si and Ge elements, and it is responsible for the high reactivity of the silicon germanide monolayer towards chemical functionalization.[32,42,43] We found that the incorporation of halogen atoms further stabilizes the SiGe monolayer. In **Table 1**, we report the formation energy per unit cell of the halogenated X2-SiGe systems that was calculated with respect to SiGe and X_2. We obtained that the halogenated X2-SiGe monolayers are between -3.0 eV and -7.3 eV more stable than the separated SiGe and X_2 species (formation energy for H2-SiGe was calculated to be -7.667 eV). In **Figure 2**, we show the calculated phonon dispersion band structures for the X2-SiGe systems. Near the Γ point we predicted a branch with imaginary frequencies of about -2 cm^{-1}. This small instability is due to the difficulty to achieve numerical convergence when using first-principles calculations for 2D materials. Even larger imaginary frequencies have been reported for the 1T′-MY_2 (M = Mo, W; Y = S, Se, Te)[44] and In_2Y_2 (Y = S, Se, Te) monolayers.[45] Thus, the dynamical stability of the 2D X2-SiGe materials is confirmed.

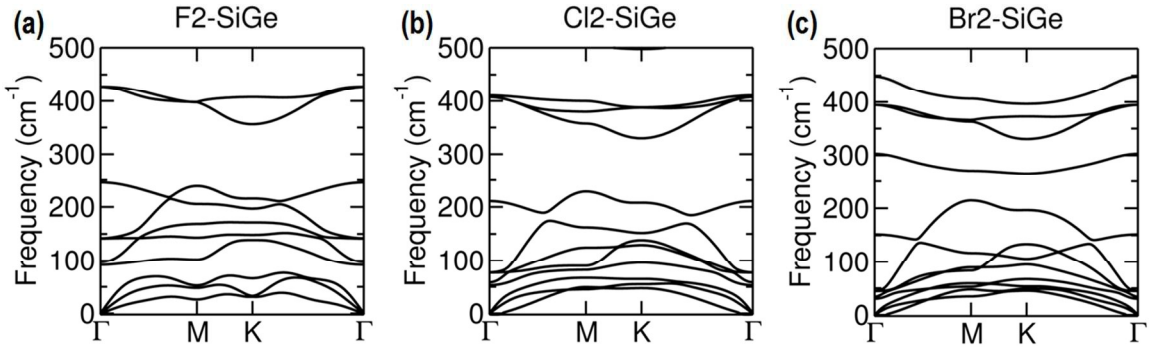

Figure 2. Phonon spectra of **(a)** F2-SiGe, **(b)** Cl2-SiGe, and **(c)** Br2-SiGe monolayers.

The electronic band structures of F2-SiGe, Cl2-SiGe and Br2-SiGe monolayers with and without SOC are plotted in **Figures 3-5**. At the ground state without including SOC, F2-

SiGe, Cl2-SiGe and Br2-SiGe have a trivial direct band gap of 0.696 eV, 0.923 eV, and 0.691 eV, respectively, which is located at the Γ point. When SOC is turned on, the band gaps are reduced by 0.05-0.1 eV. For the pristine (*i.e.*, 0% strained) X2-SiGe monolayers, the top of the valence band (VB) is characterized by the contribution of the p_x and p_y orbitals (named hereafter as p_{xy}, and represented in the plots by dark blue color), while the bottom of the conduction band (CB) is dominated by the contribution of the *s* orbital, with only small contribution of p_z (contributions from *s* orbital are represented in the plots by the red color). Under external strain without SOC, we found that the band gap of the X2-SiGe materials decreases monotonously until it becomes zero for 8% strain. The strain percentage is calculated with respect to the values of the lattice parameters at the equilibrium. Furthermore, in the 8%-strained cases, the *s* orbital at the Γ point is located below two *p* orbitals. It is known that for typical Group-4 elements based semiconductors, the *s* orbital should lie above the two *p* orbitals. This inversion between the *s* and *p* orbitals obtained for all the strained X2-SiGe systems, is a strong indication of the existence of a topological phase transition. This phenomenon was also reported earlier for distorted germanane.[25] The s-p_{xy} band inversion predicted for the strained X2-SiGe monolayers, is due to the weakening of the Si-Ge bonding that entails to reduce the difference between the energy of bonding and antibonding atomic orbitals and, consequently, leads to the shift of the *s* orbital to the occupied states below the p_{xy} orbitals. After including SOC, the degeneracy of the *p* orbitals at the Γ points is lifted and a global band gap of 53 meV, 56 meV and 123 meV is obtained for the 8%-strained F2-SiGe, Cl2-SiGe, and Br2-SiGe, respectively. In the case of H2-SiGe, this phenomenon was observed only under very high strain (> 15%) (see **Figure S1** in SI). For the I2-SiGe system, we found that the optimized structure differs from the rest of the halogenated X2-SiGe monolayers. Additionally, this material is not a semiconductor (see **Figure S2** in SI).

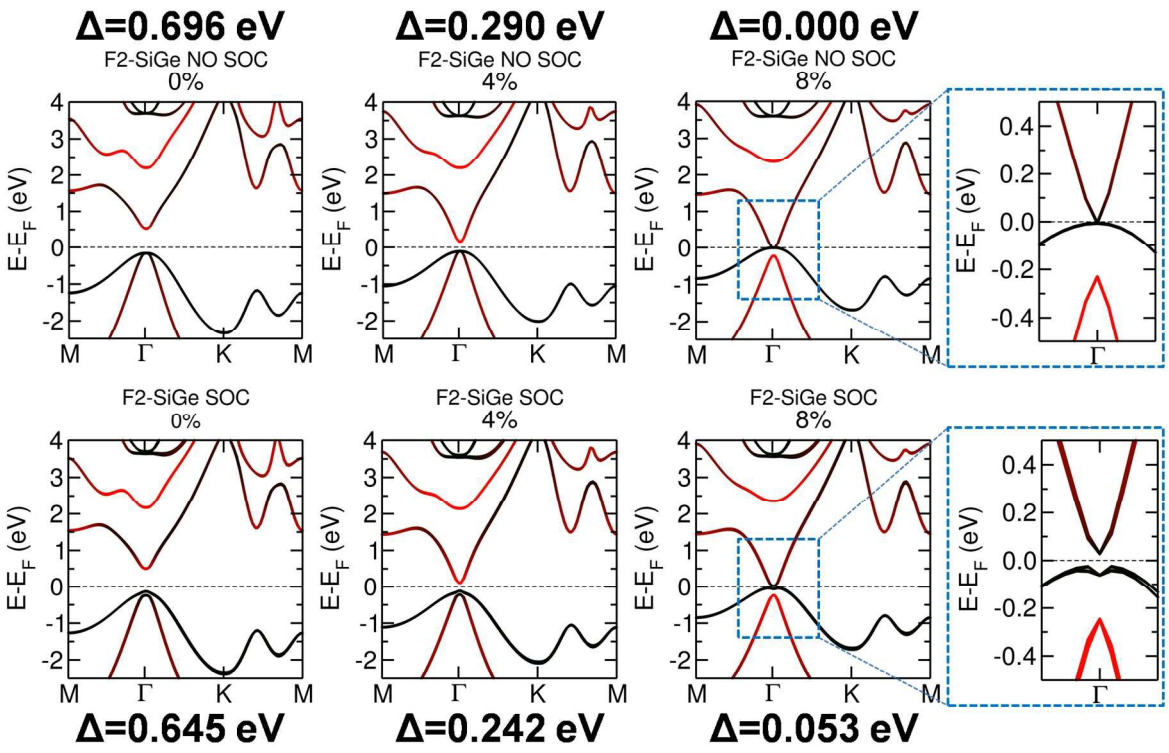

Figure 3. Evolution of the band structure of a F2-SiGe monolayer under strain. The band structures are calculated without (upper) and with (lower) SOC. The zoomed-in of the closest bands to the Fermi level for the 8%-strained F2-SiGe monolayer are shown right-most plots. Δ stands for the band gap at each percentage of strain. The color gradient indicates the contribution of the *s*, p_x, and p_y orbitals to each of the bands along the k-path – red for *s*, and dark blue for p_x, and p_y.

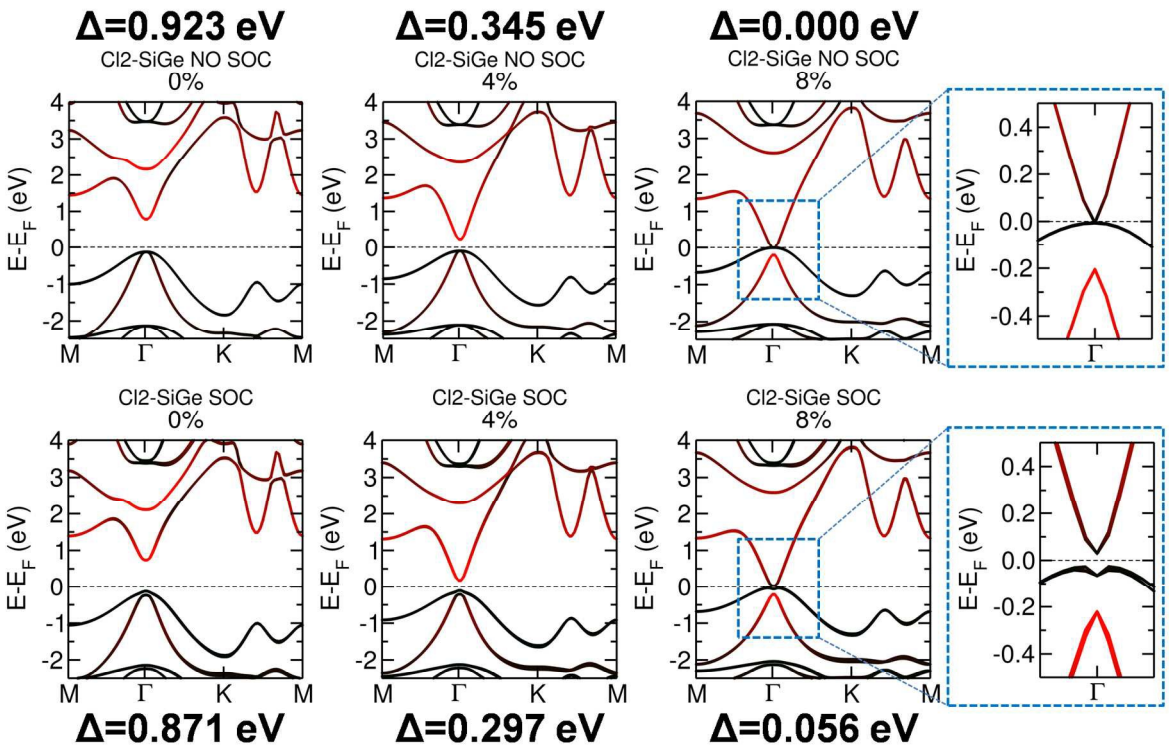

Figure 4. Evolution of the band structure of a Cl2-SiGe monolayer under strain. The band structures are calculated without (upper) and with (lower) SOC. The zoomed-in of the closest bands to the Fermi level for the 8%-strained Cl2-SiGe monolayer are shown right-most plots. Δ stands for the band gap at each percentage of strain. The color gradient indicates the contribution of the *s*, p_x, and p_y orbitals to each of the bands along the k-path – red for *s*, and dark blue for p_x, and p_y.

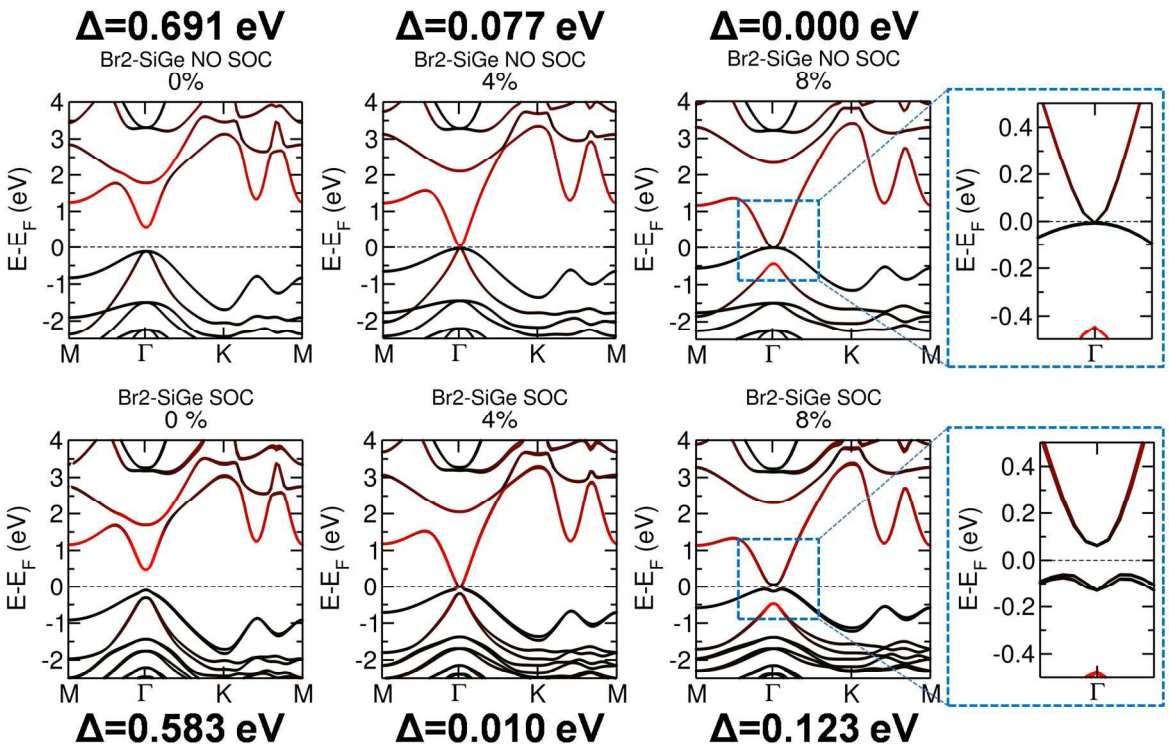

Figure 5. Evolution of the band structure of a Br2-SiGe monolayer under strain. The band structures are calculated without (upper) and with (lower) SOC. The zoomed-in of the closest bands to the Fermi level for the 8%-strained Br2-SiGe monolayer are shown right-most plots. Δ stands for the band gap at each percentage of strain. The color gradient indicates the contribution of the *s*, p_x, and p_y orbitals to each of the bands along the k-path – red for *s*, and dark blue for p_x, and p_y.

To firmly confirm the existence of topological properties in the X2-SiGe systems, we investigated the edge states of 8%-strained X2-SiGe. To this end, we used armchair nanoribbons. In these 1D models, the edges were passivated by hydrogen atoms to eliminate the dangling bonds (see **Figure 4b**). The widths of the three different nanoribbons were set to 93.25 Å (F2-SiGe), 92.56 Å (Cl2-SiGe) and 93.03 Å (Br2-SiGe), large enough to avoid the interaction between the edges. We confirm the existence of conducting edge states connecting the conduction and valence bands by a Dirac point situated at the middle of the 2D band gap (see **Figure 4a**). The placement of the Dirac point at the center of the band gap is desirable to avoid backscattering from the bulk bands, which is an important

requirement for topological insulators used in nanoelectronic devices.[6] Thus, the presence of topological edges indicate that these strained X2-SiGe monolayers are indeed 2D TIs.

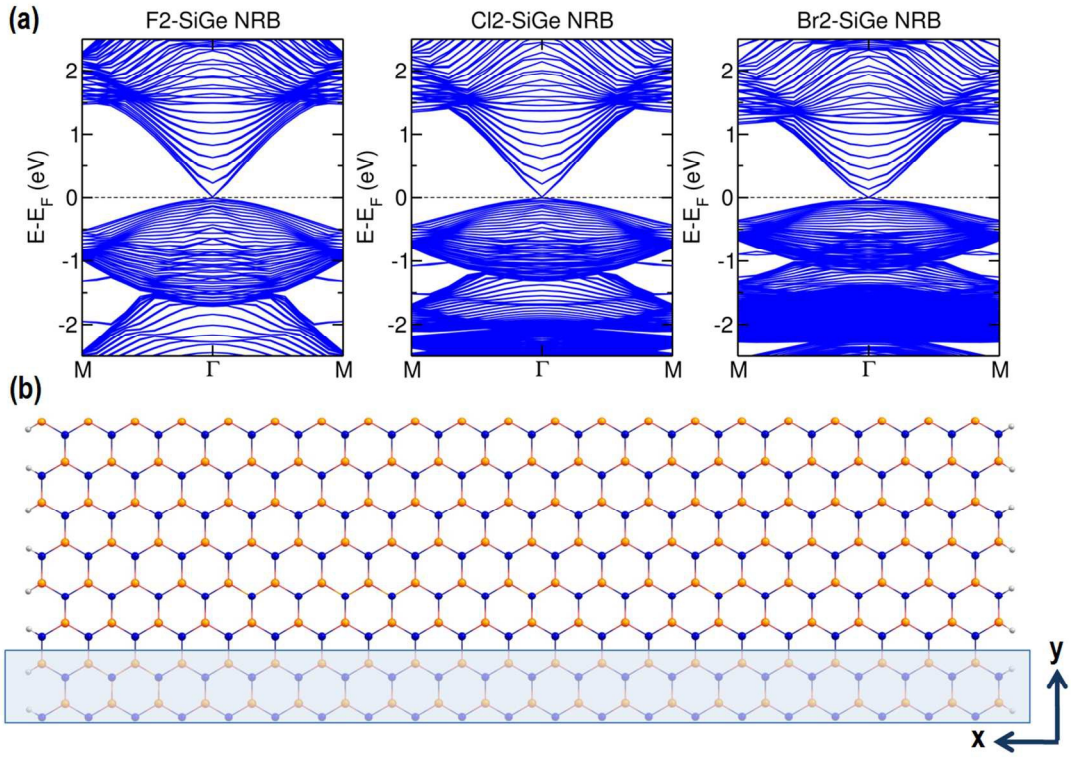

Figure 4. **(a)** Calculated edges states for strained X2-SiGe (X=F, Cl, Br) nanoribbons. **(b)** Armchair nanoribbon model used in the edge calculations. Zero of the energy is set at Fermi level. **x** and **y** indicate the width and periodicity direction of the nanoribbon, respectively.

Conclusions

Using first-principles calculations we found that functionalizing the SiGe monolayer with halogen atoms alternated on both sides of the plane, increases its stability by more than 3 eV. We found that, except for the I2-SiGe system, all the halogenated X2-SiGe monolayers are normal semiconductors with trivial band gaps that goes from 500 meV to 900 meV. Moreover, tensile strain ≥ 8% leads to TI phase transition that convert the X2-SiGe semiconductors to nontrivial topological insulators with bad gap ranging from 53 meV to 123 meV. These large SOC-induced band gaps found in the X2-SiGe systems are

promising for using these materials in spintronic and magnetoelectronic devices that operate under room temperature conditions. Interestingly, we found that the H2-SiGe monolayer also behaves as QSH insulator, but the amount of strain that has to be applied in order to observed the QSH effect is rather large (> 15%).

Acknowledgments

This work was supported by the European Research Council (ERC, StG 256962), C3ENV project. We thank Dr. Agnieszka Kuc, Dr. Augusto Oliveira and Vladimir Bačić for their support.

References

1 M. Z. Hasan and C. L. Kane, *Rev. Mod. Phys.*, 2010, **82**, 3045–3067.

2 X.-L. Qi and S.-C. Zhang, *Rev. Mod. Phys.*, 2011, **83**, 1057–1110.

3 B. A. Bernevig and S.-C. Zhang, *Phys. Rev. Lett.*, 2006, **96**, 106802.

4 C. L. Kane and E. J. Mele, *Phys. Rev. Lett.*, 2005, **95**, 226801.

5 J. E. Moore, *Nature*, 2010, **464**, 194–198.

6 S. A. Wolf, D. D. Awschalom, R. A. Buhrman, J. M. Daughton, S. von Molnár, M. L. Roukes, A. Y. Chtchelkanova and D. M. Treger, *Science*, 2001, **294**, 1488–1495.

7 Y. Yao, F. Ye, X.-L. Qi, S.-C. Zhang and Z. Fang, *Phys. Rev. B*, 2007, **75**, 41401.

8 M. König, S. Wiedmann, C. Brüne, A. Roth, H. Buhmann, L. W. Molenkamp, X.-L. Qi and S.-C. Zhang, *Science*, 2007, **318**, 766–770.

9 I. Knez, R.-R. Du and G. Sullivan, *Phys. Rev. Lett.*, 2011, **107**, 136603.

10 T. Hirahara, G. Bihlmayer, Y. Sakamoto, M. Yamada, H. Miyazaki, S. Kimura, S. Blügel and S. Hasegawa, *Phys. Rev. Lett.*, 2011, **107**, 166801.

11 S. H. Kim, K.-H. Jin, J. Park, J. S. Kim, S.-H. Jhi, T.-H. Kim and H. W. Yeom, *Phys. Rev. B*, 2014, **89**, 16801.

12 C. Sabater, D. Gosálbez-Martínez, J. Fernández-Rossier, J. G. Rodrigo, C. Untiedt and J. J. Palacios, *Phys. Rev. Lett.*, 2013, **110**, 176802.

13 I. K. Drozdov, A. Alexandradinata, S. Jeon, S. Nadj-Perge, H. Ji, R. J. Cava, B. Andrei Bernevig and A. Yazdani, *Nat Phys*, 2014, **10**, 664–669.

14 A. Takayama, T. Sato, S. Souma, T. Oguchi and T. Takahashi, *Phys. Rev. Lett.*, 2015, **114**, 66402.

15 N. Kawakami, C.-L. Lin, M. Kawai, R. Arafune and N. Takagi, *Appl. Phys. Lett.*, 2015, **107**, 031602.

16 F. Yang, L. Miao, Z. F. Wang, M.-Y. Yao, F. Zhu, Y. R. Song, M.-X. Wang, J.-P. Xu, A. V Fedorov, Z. Sun, G. B. Zhang, C. Liu, F. Liu, D. Qian, C. L. Gao and J.-F. Jia, *Phys. Rev. Lett.*, 2012, **109**, 16801.

17 S. Murakami, *Phys. Rev. Lett.*, 2006, **97**, 236805.

18 F.-C. Chuang, L.-Z. Yao, Z.-Q. Huang, Y.-T. Liu, C.-H. Hsu, T. Das, H. Lin and A. Bansil, *Nano Lett.*, 2014, **14**, 2505–2508.

19 J.-J. Zhou, W. Feng, C.-C. Liu, S. Guan and Y. Yao, *Nano Lett.*, 2014, **14**, 4767–4771.

20 Y. Ma, Y. Dai, L. Kou, T. Frauenheim and T. Heine, *Nano Lett.*, 2015, **15**, 1083–1089.

21 C.-C. Liu, H. Jiang and Y. Yao, *Phys. Rev. B*, 2011, **84**, 195430.

22 Y. Ma, Y. Dai, C. Niu and B. Huang, *J. Mater. Chem.*, 2012, **22**, 12587–12591.

23 C.-C. Liu, W. Feng and Y. Yao, *Phys. Rev. Lett.*, 2011, **107**, 76802.

24 Y. Ma, Y. Dai, W. Wei, B. Huang and M.-H. Whangbo, *Sci. Rep.*, 2014, **4**, 7297.

25 C. Si, J. Liu, Y. Xu, J. Wu, B.-L. Gu and W. Duan, *Phys. Rev. B*, 2014, **89**, 115429.

26 X. Qian, J. Liu, L. Fu and J. Li, *Science*, 2014, **346**, 1344–1347.

27 R. Pachavis, *III-V and IV-IV Materials and Processing Challenges for Highly Integrated Microelectronics and Optoelectronics, MRS Symposium Volume 535*, Material s Research Society, U.S. Army Research Office P.O.Box 12211 Research Triangle Park, NC 27709-2211, 1999.

28 E. Bianco, S. Butler, S. Jiang, O. D. Restrepo, W. Windl and J. E. Goldberger, *ACS Nano*, 2013, **7**, 4414–4421.

29 K. J. Koski and Y. Cui, *ACS Nano*, 2013, **7**, 3739–3743.

30 S. Jiang, S. Butler, E. Bianco, O. D. Restrepo, W. Windl and J. E. Goldberger, *Nat. Commun.*, 2014, **5**, 1–4.

31 F. Zhu, W. Chen, Y. Xu, C. Gao, D. Guan, C. Liu, D. Qian, S.-C. Zhang and J. Jia, *Nat. Mater.*, 2015, **14**, 1020–1025.

32 H. Zhou, M. Zhao, X. Zhang, W. Dong, X. Wang, H. Bu and A. Wang, *J. Phys. Condens. Matter.*, 2013, **25**, 395501.

33 M. Houssa, E. Scalise, K. Sankaran, G. Pourtois, V. V Afanas'ev and A. Stesmans, *Appl. Phys. Lett.*, 2011, **98**, 223107.

34 X.-Q. Wang, H.-D. Li and J.-T. Wang, *Phys. Chem. Chem. Phys.*, 2012, **14**, 3031–3036.

35 W. Kohn and L. J. Sham, *Phys. Rev.*, 1965, **140**, A1133–A1138.

36 J. P. Perdew, K. Burke and M. Ernzerhof, *Phys. Rev. Lett.*, 1996, **77**, 3865–3868.

37 P. Hohenberg and W. Kohn, *Phys. Rev.*, 1964, **136**, B864–B871.

38 G. Kresse and D. Joubert, *Phys. Rev. B*, 1999, **59**, 1758–1775.

39 G. Kresse and J. Furthmüller, *Phys. Rev. B*, 1996, **54**, 11169–11186.

40 H. J. Monkhorst and J. D. Pack, *Phys. Rev. B*, 1976, **13**, 5188–5192.

41 P. Giannozzi, S. Baroni, N. Bonini, M. Calandra, R. Car, C. Cavazzoni, D. Ceresoli, G. L. Chiarotti, M. Cococcioni, I. Dabo, A. D. Corso, S. de Gironcoli, S. Fabris, G. Fratesi, R. Gebauer, U. Gerstmann, C. Gougoussis, A. Kokalj, M. Lazzeri, L. Martin-Samos, N. Marzari, F. Mauri, R. Mazzarello, S. Paolini, A. Pasquarello, L. Paulatto, C. Sbraccia, S. Scandolo, G. Sclauzero, A. P. Seitsonen, A. Smogunov, P. Umari and R. M. Wentzcovitch, *J. Phys.: Condens. Matter*, 2009, **21**, 395502–1–19.

42 B. van den Broek, M. Houssa, E. Scalise, G. Pourtois, V. V Afanas'ev and A. Stesmans, *Appl. Surf. Sci.*, 2014, **291**, 104–108.

43 P. A. Denis, *Phys. Chem. Chem. Phys.*, 2015, **17**, 5393–5402.

44 D. B. Putungan, S.-H. Lin and J.-L. Kuo, *Phys. Chem. Chem. Phys.*, 2015, **17**, 21702–21708.

45 V. Zólyomi, N. D. Drummond and V. I. Fal'ko, *Phys. Rev. B*, 2014, **89**, 205416–1–8.